

---

## Heat Transfer Coefficients during Quenching of Steels

H. S. Hasan · M. J. Peet · J. M. Jalil · H.  
K. D. H. Bhadeshia

**Abstract** Heat transfer coefficients for quenching in water have been measured as a function of temperature using steel probes for a variety of iron alloys. The coefficients were derived from measured cooling curves combined with calculated heat-capacities. The resulting data were then used to calculate cooling curves using the finite volume method for a large steel sample and these curves have been demonstrated to be consistent with measured values for the large sample. Furthermore, by combining the estimated cooling curves with time-temperature-transformation diagrams it has been possible to predict the variation of hardness as a function of distance via the quench factor analysis. The work should prove useful in the heat treatment of the steels studied, some of which are in the development stage.

**Keywords** heat transfer coefficient · steel · hardness prediction · phase transformation

---

H. S. Hasan  
The University of Technology, Baghdad  
Department of Electromechanical Engineering  
Baghdad, Iraq

M. J. Peet  
University of Cambridge  
Department of Materials Science and Metallurgy  
Pembroke Street, Cambridge CB2 3QZ, U. K.

J. M. Jalil  
The University of Technology, Baghdad  
Department of Electromechanical Engineering  
Baghdad, Iraq

H. K. D. H. Bhadeshia (corresponding author)  
University of Cambridge  
Department of Materials Science and Metallurgy  
Pembroke Street, Cambridge CB2 3QZ, U. K.  
E-mail: hkdb@cam.ac.uk

---

## 1 Introduction

Quenching is a widely used commercial process in which steel components in their austenitic state are immersed in a liquid at a much lower temperature, resulting in rapid cooling, and under appropriate circumstances, the hardening of the steel. This simple description hides the complexity of the process, in which the transfer of heat to the quenching medium involves many phenomena at the steel/liquid interface (which may enclose a vapour gap), some of which are expressed in terms of a heat-transfer coefficient ( $h$ ) which is a function of the steel and quenchant. The heat flux across the interface is given by  $q = h\Delta T$  where  $\Delta T$  is the temperature difference between the source and the sink. The heat transfer coefficient is often approximated to be constant, and this may be valid over specified temperature ranges. However, it can vary significantly with temperature [22], in which case a reliable estimation of the cooling behaviour of a quenched component, and any subsequent calculations of structure and properties, requires accurate and temperature-dependent heat transfer coefficients [8, 25, 27].

The heat transfer coefficient can be measured experimentally using a cylindrical probe with one or more thermocouples attached. The probe is quenched and the variation in temperature as a function of time is measured [2, 16, 21] and the resulting data interpreted in order to determine  $h$ . The probe diameter is usually in excess of 12.5 mm, with a length at least four times the diameter in order to minimise end-cooling effects. The probes are usually made from metals which do not undergo phase transformations, such as Inconel 600 [7, 9, 12, 19], silver [12] or austenitic steel [10, 30]. This avoids the influence of enthalpy changes due to phase transformations; by the same logic, it does not reveal the effect of such changes on the heat-transfer coefficient, which may be important since the majority of heat-treatments are conducted on transforming steels.

The purpose of the present work was to undertake detailed measurements of the heat-transfer coefficients of a number of transforming steels, and to combine the data thus collected with a variety of mathematical models to enable the prediction of the hardness following the quenching heat-treatments.

## 2 Method

Equipment was designed consisting of a data-acquisition system, a small tube furnace, a  $\frac{1}{4}$  l beaker containing the quenchant and K-type thermocouple, Fig. 1. The probe material was, after machining, cleaned in an ultrasonic bath containing methanol. The 1 mm diameter thermocouple was inserted into the cylindrical probe together with some fine graphite powder for better thermal contact. It was held in position using a screw from the side and any gap between the probe and thermocouple sealed using alumina paste which was furnace-hardened for 8 h at 200°C in order to avoid erroneous readings from the leakage of quenchant into the thermocouple. The probe assembly was placed vertically into a tube furnace with a hot-zone of 13 cm, through a guide-hole and held at 850°C for 5 min before allowing the probe to fall and be brought to a standstill by the flange when it enters the quenchant in the beaker. The quenchant volume is sufficiently large to ensure no significant change in its temperature due to the quench. Throughout this process, data were collected on a computer at a rate of 1000 temperature readings per second.

The probe dimensions were determined by calculating the Biot number,  $Bi = hL/k \leq 0.1$ , where  $L$  is the characteristic length and  $k$  the thermal conductivity. The latter is typically  $50 \text{ W m}^{-1} \text{ K}^{-1}$  and assuming a heat transfer coefficient of  $10^4 \text{ W m}^{-2} \text{ K}^{-1}$  permits the estimation of the required length of the probe. The condition that  $Bi \leq 0.1$  is equivalent to assuming that the controlling heat-transfer resistance is confined to the external coolant, and the establishment of quasi-flat temperature profiles inside the sample [1]. The probe length is five times its diameter in so that end-effects can be neglected and to justify the assumption that only radial heat-flow occurs at its half-length. The surface finish of the probe was fixed by machining and grinding.

The probe materials investigated are listed in Table 1; they were selected from available alloys to cover a range of carbon concentrations and hardenabilities; alloy C is from a new class of bulk nanostructured-steels which transform at very low homologous temperatures [6].

All reported hardness determinations used a 30 kg load and the values quoted are averages from a minimum of 3 indents.

**Table 1** Chemical compositions of the probe materials in wt%.

Steel	C	Si	Mn	Ni	Mo	Cr	Al	Co	Cu
A	0.16	0.16	0.67	0.08	0.02	0.06	-	-	-
B	0.15	1.19	1.50	0.08	0.31	1.19	0.02	-	0.136
C	0.78	1.60	2.02	-	0.25	1.01	1.37	3.87	-
D	0.55	0.22	0.77	0.15	0.05	0.20	-	-	-
E	0.54	0.20	0.74	0.17	0.05	0.20	-	-	-
F	0.16	0.22	0.30	2.93	0.39	1.47	0.28	-	0.01

### 3 Data Analysis and Results

A minimum of three quenching experiments were performed in each case to assess repeatability. To reduce the influence of noise, the time-temperature data were smoothed using a rolling average of 11 points in order to calculate the cooling rate by differentiation. The temperature-dependent heat-transfer coefficient is then given by [17, 18, 23]:

$$h = \frac{\rho V C_P \dot{T}}{A(T_S - T_\infty)} \quad (1)$$

where  $C_P$  is the specific heat capacity at constant pressure,  $V$  and  $A$  the sample volume and surface area respectively,  $\rho = 7858 \text{ kg m}^{-3}$  the density which is assumed to be constant, and  $\dot{T}$  the instantaneous cooling rate. The heat capacity was calculated as a function of temperature using the thermodynamic software MTDATA [24] with the SGTE database, for the steel in the austenitic state since the alloys were expected to remain untransformed until the martensite-start ( $M_S$ ) temperature is reached. Typical results for alloy D are illustrated in Fig. 2. The data for equilibrium mixtures of ferrite and cementite are also plotted because as will be seen later, the largest of samples do

not completely transform into martensite; in such cases, the equilibrium calculation represents an upper limit for the heat capacity. Fig. 3 shows the measured cooling and cooling-rate curves for alloy D, together with the derived heat transfer coefficient as a function of surface temperature. The readings below about 100°C become noisy because the difference in temperature between adjacent recordings becomes comparable to the accuracy of the thermocouple. These curves are, over the temperature range 600–850°C, typical of all the experiments and the complete set is illustrated in Fig. 4.

However, there are important differences with respect to alloys A and C, both of which have exhibited a high cooling rate during the quench at temperatures below about 400°C, Fig. 4a. Alloy A does not have sufficient hardenability in order to ensure a fully martensitic microstructure on quenching (Fig. 5a); the sample has a hardness of only 260HV in its final state (Table 2). Allotriomorphic ferrite forms at high temperatures, so that the amount of austenite which undergoes martensitic transformation is reduced, resulting in a smaller enthalpy change and hence a faster cooling rate (relative to those alloys which become fully martensitic) at low temperatures during the quench. In the case of alloy C, the hardenability is sufficient to yield a martensitic microstructure (Fig. 5b) with a hardness of 730 HV, but calculations using MTDATA revealed that the enthalpy change at the  $M_S = 202^\circ\text{C}$  for alloy C is  $\Delta H = 4600 \text{ J mol}^{-1}$ , which compares with  $\Delta H = 6000\text{--}7000 \text{ J mol}^{-1}$  for the other steels, Fig. 6. The smaller release in heat on transformation is consistent with the more rapid cooling rate at low temperatures for alloy C.

**Table 2** Vickers hardness data measured using a 30 kg load following quenching. The maximum hardness refers to samples that were quenched into agitated water at 20°C, after austenitisation at 950°C for 30 min; these values are necessary in the quench factor analysis. The martensite-start temperatures are calculated using a neural network based on the data from [29].

Steel	$M_S/^\circ\text{C}$	Probe hardness	Maximum Hardness
A	455	260±9	351±8
B	435	456±34	471±6
C	202	753±2	748±7
D	269	728±13	731±1
E	276	735±15	720±6
F	405	458±7	473±13

#### 4 Application of Heat Transfer Coefficients

The work presented below was done to demonstrate the utility of the measured heat-transfer coefficients for samples bigger than the probes described earlier and for the Fe-0.55 wt%, steel D, Table 1). A large cylinder, 52 mm diameter, 20 mm long was instrumented with three thermocouples placed in 1 mm diameter axial holes drilled 10 mm into the sample. The holes were located at the centre of the cylinder, about 0.5 mm from the surface, and half way along its radius. The sample was then austenitised and quenched into water while recording the cooling curves.

The measured cooling curves were compared against those calculated using discretised heat flow equations based on a finite volume method described elsewhere in detail [14, 28]. The calculations require a knowledge of the density, thermal conductivity (obtained from a neural network model [15]), and the relevant measured heat transfer coefficients (Fig. 4). The heat capacity was once again calculated as a function of temperature using MTDATA, allowing ferrite, cementite and austenite to exist (Fig. 2); the peak in capacity that occurs at the Curie temperature was truncated by describing the variation using a polynomial equation in order to avoid computational difficulties [13].

The calculated and measured curves are presented in Fig. 7. There is reasonable agreement except at the very surface, and there seems to be some influence of the latent heat of transformation on the measured curves, which has not been taken into account in the calculations. The microstructure of the sample was characterised metallographically and ranged from martensite near the surface to a mixture of ferrite and pearlite at the centre (the micrographs are omitted for brevity).

It is possible to use the cooling information to calculate the variation in hardness because in *quench factor* analysis there is a correlation between the cooling curve and a property of interest (in this case hardness). Quench factor analysis was originally proposed by Evancho and Staley [11] and has since then been justified and developed further; a recent paper [26] is a good summary of its modern interpretation. In essence, the variation of the normalised value of hardness is expressed in terms of the quench factor  $Q$  as:

$$\frac{H - H_{min}}{H_{max} - H_{min}} = \exp\{k_1 Q\} \quad \text{with} \quad Q = \int_{t_o}^{t_f} \frac{dt}{t_C} \quad (2)$$

where  $H$  is the hardness and the subscripts represent minimum and maximum values of the hardness, and  $k_1$  represents the logarithm of the fraction of transformation.  $t_C$  represents the critical time required to achieve a given fraction of phase transformation. The maximum hardness is taken to be that of martensite, measured by quenching a 4 mm sample of the steel into water following austenitisation at 950°C for 30 min. This was confirmed to give a fully martensitic microstructure with a hardness  $H_{max} = 731$  HV. The value of  $H_{min}$  was obtained by similarly austenitising but then transforming isothermally at 650°C for 2 h in order to obtain pearlite with a hardness of 185 HV. There was no significant scatter observed in these values, which were constant within  $\pm 1$  HV.

Time–temperature transformation (TTT) diagrams were calculated for steel D using the thermodynamic and kinetic methods described in [3–5]<sup>1</sup>. The calculation is illustrated in Fig. 8a with the imposed calculated cooling curves. The TTT curves represent the onset of transformation, the first detectable quantity, taken to represent 0.05 fraction of reaction, the logarithm of which gives  $k_1$ . Fig. 8b shows the comparison between the calculated and measured hardness values, with good agreement given the lack of assumptions in the analysis. Further improvements may be possible by better accounting for the latent heat of transformation and specific heat capacity. How-

<sup>1</sup> The software for doing these calculations is available freely on

ever, this is not trivial because it would be necessary to have a coupling with detailed phase transformation models to represent the evolution of microstructure.

In the present work we have used steel probes to determine the heat-transfer coefficients given that the interest is in the heat-treatment of iron alloys. Fig. 9a shows  $h$  measured in the present work using the steel probe for steel D, and data from the literature on the JIS and Inconel 600 probes [20]. Fig. 9 shows that better agreement is obtained using the heat transfer coefficients determined using the steel probe.

## 5 Conclusions

1. A probe has been developed to determine the heat transfer coefficient of steel. The probe dimensions were fixed by ensuring an appropriate Biot number so that the probe temperature can be as uniform as possible during the course of the experiments.
2. The confidence in the measured heat transfer coefficients is supported by the fact that reasonable predictions could be made of the cooling curves when applied to a steel sample much larger than the probes.
3. The heat-transfer coefficients when combined with calculated cooling and time-temperature-transformation curves, can with the help of the quench factor method enable the estimation of hardness variation as a function of distance.
4. It has been demonstrated that the steel probe, which replicates phase transformations during the course of cooling, is the best for determining the heat-transfer coefficients.

**Acknowledgements** The authors are grateful to British Universities Iraq Consortium for funding this work, to the Ministry of Education in Iraq and to the University of Cambridge for the provision of laboratory facilities.

## References

1. Arpaci VS (1966) Conduction heat transfer. Addison-Wesley Publication Company, Reading, Massachusetts, USA
2. Bates CE, Totten GE, Clinton NA (1993) Handbook of Quenchants and Quenching Technology. ASM International, Materials Park, Ohio, USA
3. Bhadeshia HKDH (1981) The driving force for martensitic transformation in steels. *Metal Science* 15:175–177
4. Bhadeshia HKDH (1981) Thermodynamic extrapolation and the martensite-start temperature of substitutionally alloyed steels. *Metal Science* 15:178–150
5. Bhadeshia HKDH (1982) A thermodynamic analysis of isothermal transformation diagrams. *Metal Science* 16:159–165
6. Caballero FG, Bhadeshia HKDH, Mawella KJA, Jones DG, Brown P (2002) Very strong, low-temperature bainite. *Materials Science and Technology* 18:279–284
7. Chen N, Zhang W, Gao C, Liao B, Pan J (2006) The effects of probe geometric shape on the cooling rate curves obtained from different quenchants. *Diffusion and defect data Solid state data Part B, Solid state phenomena* 118:227–231
8. Chen N, Han L, Zhang W, Hao X (2007) Enhancing mechanical properties and avoiding cracks by simulation of quenching connecting rods. *Materials Letters* 61:3021–3024

- 
9. Chen N, Han L, Zhang W, Hao X (2007) Enhancing mechanical properties and avoiding cracks by simulation of quenching connecting rods. *Materials Letters* 61:3021–3024
  10. Chen X, Meekisho L, Totten GE (1999) Computer-aided analysis of the quenching probe test. In: Wallis RA, Walton HW (eds) *Heat Treating: Proceedings of the 18th Conference*, ASM International, Materials Park, Ohio, USA
  11. Evancho JW, Stanley JT (1974) Kinetics of precipitation in aluminium alloys during continuous cooling. *Metallurgical Transactions* 5:43–47
  12. Funatani K, Narazaki M, Tanaka M (1999) Comparisons of probe design and cooling curve analysis methods. In: Midea SJ, Pfaffmann GD (eds) *19th ASM Heat Treating Society Conference*, ASM International, Materials Park, Ohio, USA, pp 255–263
  13. Goldak J, Bibby M, Moore J, House R, Patel B (1986) Computer modeling of heat flow in welds. *Metallurgical Transactions B* 17:587–600
  14. Hasan HS (2009) Heat transfer and phase transformations in steels. PhD thesis, University of Technology, Baghdad, Baghdad, Iraq
  15. Hasan HS, Peet M (2009) Map\_steel\_thermal. Computer program <http://www.msm.cam.ac.uk/map/steel/programs/thermalmodel.html>, University of Cambridge
  16. Hernández-Morales B, Téllez-Martinez JS, Ingalls-Cruz A, Godlínz JB (1999) Cooling curve analysis using an interstitial-free steel probe. In: Midea SJ, Pfaffmann GD (eds) *Heat Treating: Proceedings of the 19th Conference*, ASM International, Materials Park, Ohio, USA, pp 284–291
  17. Holman JP (2004) *Heat Transfer*. McGraw Hill, New York, USA
  18. Kreith F (ed) (1999) *Mechanical Engineering Handbook*. CRC Press LLC, Florida, USA
  19. Ksenofontov AG, Shevchenko SY (1998) Zak-PG polymer quenching medium. *Metal Science and Heat Treatment* 40:9–10
  20. Liscic B, Tensi HM, Luty W (1992) *Theory and technology of quenching*. Springer-Verlag, Berlin, Germany
  21. Ma S, Varde AS, Takahashi M, Rondeau DK, Maniruzzaman M, Jr RDS (2003) Quenching – understanding, controlling and optimising the process. In: *4th International Conference on Quenching and the Control of Distortion*, ASM International, Materials Park, Ohio, USA
  22. Murakawa H, Beres M, Vega A, Rashed S, Davies CM, Dye D, Nikbin MK (2008) Effect of phase transformation onset temperature on residual stress in welded thin steel plates. *Transactions of JWRI* 37:75–80
  23. Myers GE (1971) *Analytical methods in conduction heat transfer*. McGraw Hill, New York, USA
  24. NPL (2006) MTDATA. Software, National Physical Laboratory, Teddington, U.K.
  25. Penha RN, Canale LC, Totten GE, Sarmiento GS, Ventura JM (2006) Effect of vegetable oil oxidation on the ability to harden AISI 4140 steel. *Journal of ASTM International* 3:89–97
  26. Rometsch P, Starink M, Gregson P (2003) Improvements in quench factor modelling. *Materials Science & Engineering A* 339:255–264
  27. Smith DE (1999) Computing the heat transfer coefficients for industrial quenching processes. In: Midea SJ, Pfaffmann GD (eds) *Heat Treating: Proceedings of the 19th Conference*, ASM International, Materials Park, Ohio, USA, pp 325–334

28. Smoljan B (2006) Prediction of mechanical properties and microstructure distribution of quenched and tempered steel shaft. *Journal of Materials Processing Technology* 175:393–397
29. Sourmail T, Garcia-Mateo C (2005) A model for predicting the martensite–start temperature of steels. *Computational Materials Science* 34:213–218
30. Totten GE, Sun YH, Bates CE (2000) Simplified property predictions for AISI 1045 based on quench factor analysis. In: Midea SJ, Pfaffmann GD (eds) 19th ASM Heat Treating Society Conference and Exposition including Steel Heat Treating in the New Millenium, ASM International, Materials Park, Ohio, USA, pp 292–298

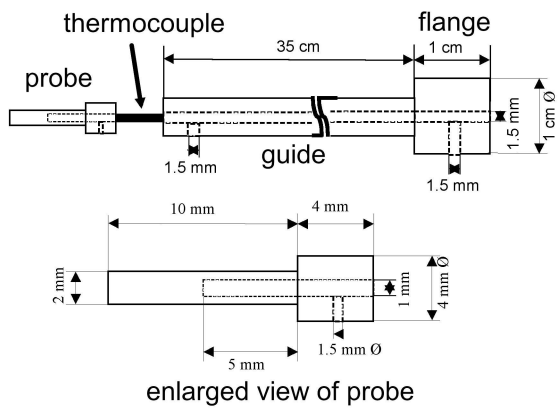


**Fig. 1** Design of the probe and thermocouple assembly.

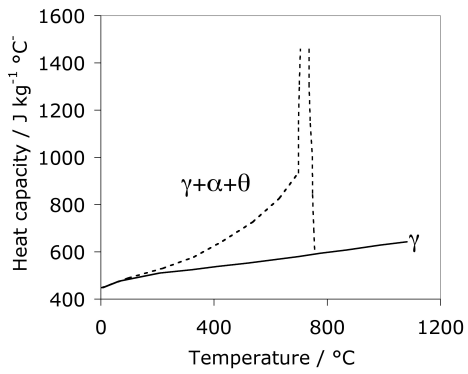


**Fig. 2** Calculated specific heat capacity for steel D as a function of temperature.  $\gamma$ ,  $\alpha$  and  $\theta$  refer to austenite, ferrite and cementite respectively.

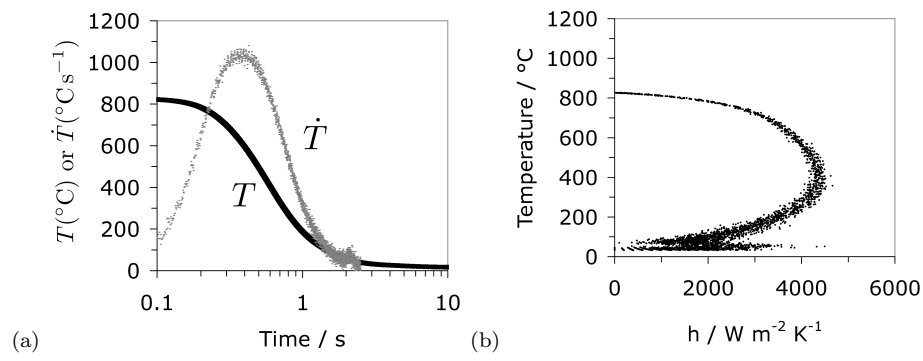


**Fig. 3** Alloy D. (a) Temperature and derived values of cooling rate as a function of time. (b) Corresponding calculated heat-transfer coefficient as a function of temperature. The values below about 100°C should be neglected due to noise in the measurement of the cooling curve.

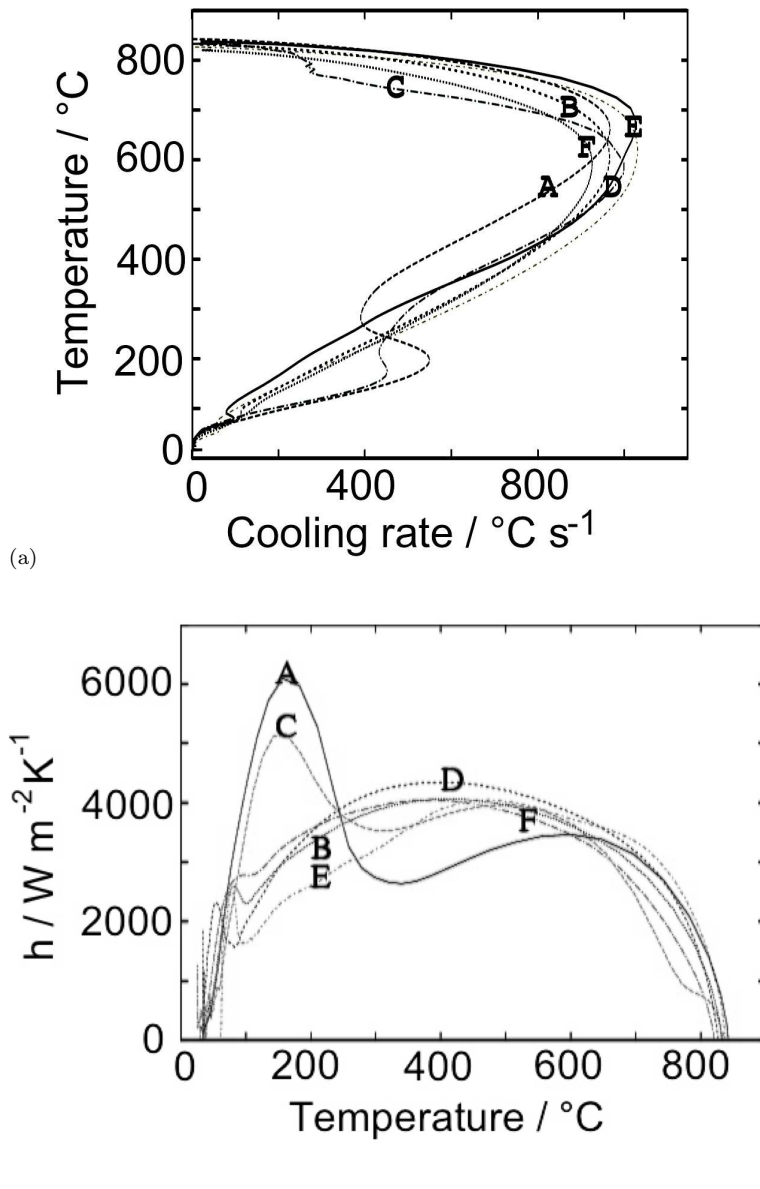


**Fig. 4** (a) Cooling curves recorded for all steels. (b) A summary of the derived heat transfer coefficients for all the alloys listed in Table 1.

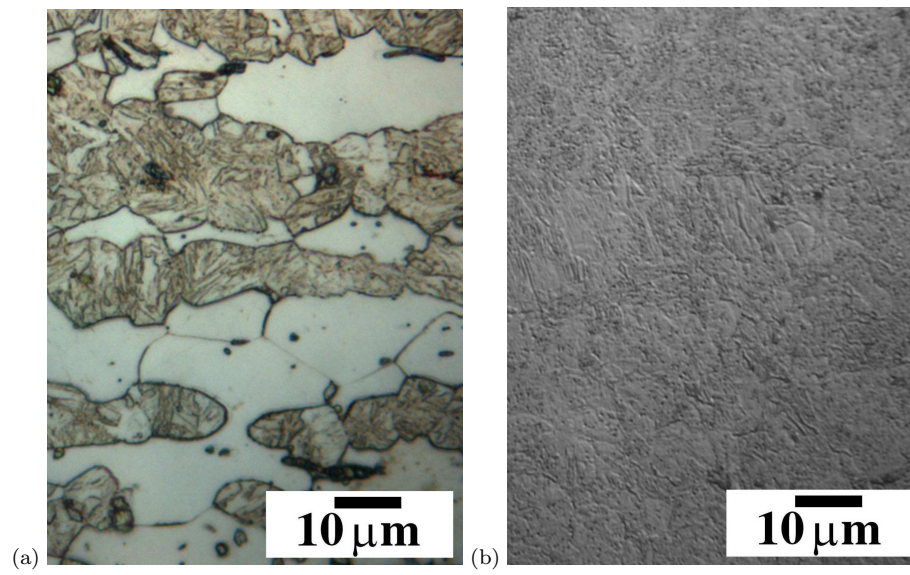


**Fig. 5** Optical micrographs from the quenched state. (a) Steel A, showing a mixture of allotriomorphic ferrite and martensite. (b) Steel C, showing a martensitic microstructure with traces of retained austenite. The other steels were examined metallographically but were fully martensitic and micrographs are not included here for the sake of brevity.

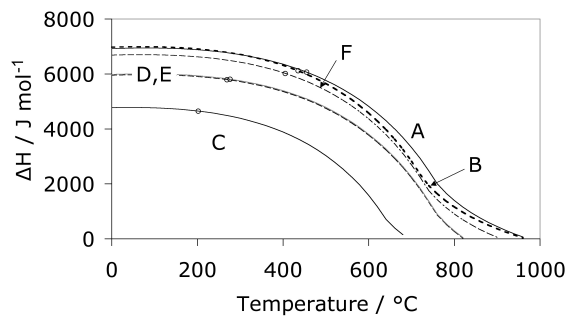


**Fig. 6** Calculated enthalpy change for austenite transforming to ferrite of the same chemical composition, as a function of temperature. The  $M_S$  temperature for each steel is also plotted as circles.

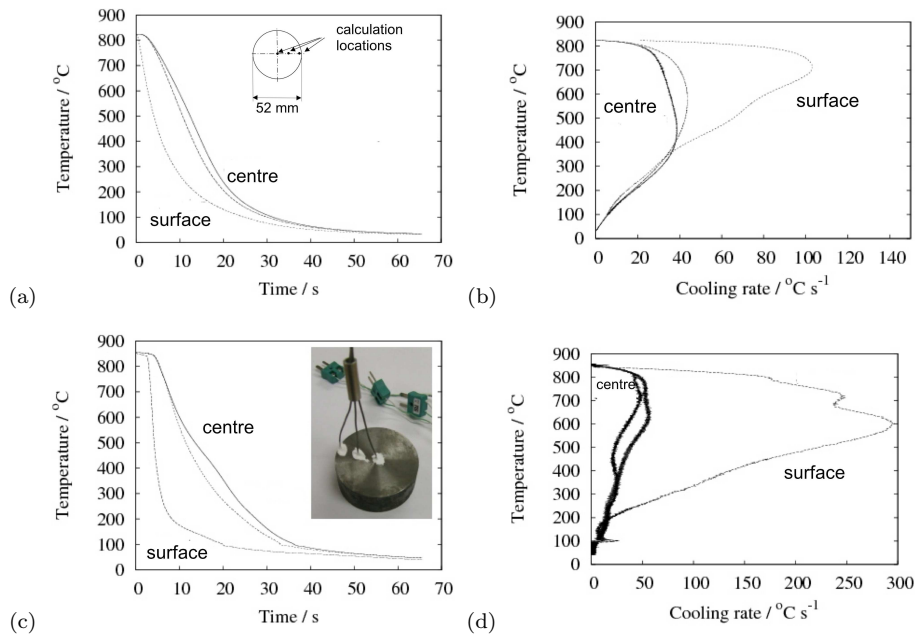


**Fig. 7** (a) Calculated cooling curve. (b) Calculated cooling rates. (c) Measured cooling curve. The inset shows the sample used. (d) Measured cooling rates.

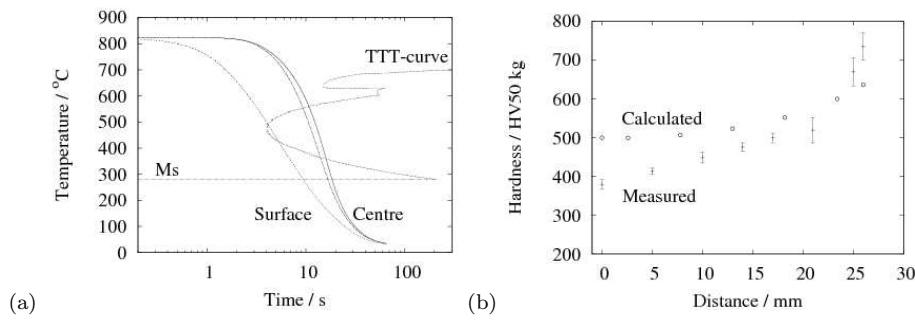


**Fig. 8** (a) Calculated data. (b) Comparison between calculated and measured hardness values.

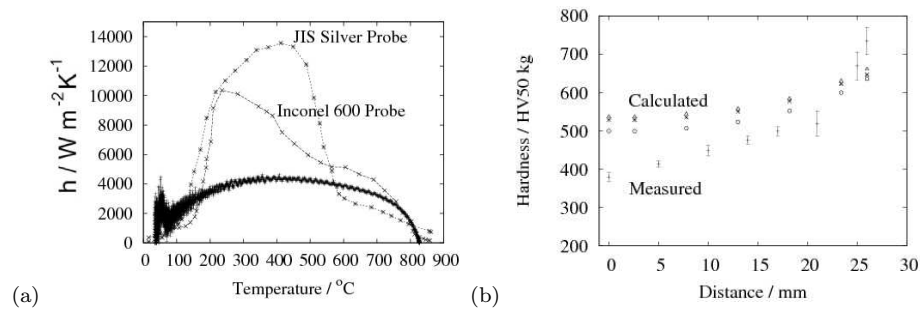


**Fig. 9** (a) Heat transfer coefficients for different probes. (b) Comparison between calculated and measured hardness values. The top and middle sets of points represent the Inconel and JIS probes respectively, and the measured values the steel probe used in the present work.